







Effect of nodule size and stiffness on phonation threshold and collision pressures in a synthetic hemilaryngeal vocal fold model

Mohsen Motie-Shirazi,¹  Matías Zañartu,²  Sean D. Peterson,³  Daryush D. Mehta,⁴ 
 Robert E. Hillman,⁴  and Byron D. Erath^{1,a)} 

¹Department of Mechanical and Aerospace Engineering, Clarkson University, Potsdam, New York 13699, USA

²Department of Electronic Engineering, Universidad Técnica Federico Santa María, Valparaíso, Chile

³Department of Mechanical and Mechatronics Engineering, University of Waterloo, Waterloo, Ontario, Canada

⁴Center for Laryngeal Surgery and Voice Rehabilitation, Massachusetts General Hospital, Boston, Massachusetts 02114, USA

ABSTRACT:

Synthetic vocal fold (VF) replicas were used to explore the role of nodule size and stiffness on kinematic, aerodynamic, and acoustic measures of voiced speech production. Emphasis was placed on determining how changes in collision pressure may contribute to the development of phonotrauma. This was performed by adding spherical beads with different sizes and moduli of elasticity at the middle of the medial surface of synthetic silicone VF models, representing nodules of varying size and stiffness. The VF models were incorporated into a hemilaryngeal flow facility. For each case, self-sustained oscillations were investigated at the phonation threshold pressure. It was found that increasing the nodule diameter increased the open quotient, phonation threshold pressure, and phonation threshold flow rate. However, these values did not change considerably as a function of the modulus of elasticity of the nodule. Nevertheless, the ratio of collision pressure to subglottal pressure increased significantly for both increasing nodule size and stiffness. This suggests that over time, both growth in size and fibrosis of nodules will lead to an increasing cycle of compensatory vocal hyperfunction that accelerates phonotrauma.

© 2023 Acoustical Society of America. <https://doi.org/10.1121/10.0016997>

(Received 27 May 2022; revised 19 December 2022; accepted 6 January 2023; published online 27 January 2023)

[Editor: Zhaoyan Zhang]

Pages: 654–664

I. INTRODUCTION

Nodules are benign vocal fold (VF) lesions that usually protrude from the border of the anterior and middle third of the medial surface of the VFs.¹ They are commonly bilateral and are believed to be caused by repetitive VF trauma,^{2,3} which can arise due to vocal hyperfunction.^{4–7} The presence of VF nodules can disrupt VF oscillations and, consequently, negatively impact phonation.^{8,9}

Phonotraumatic vocal hyperfunction can create excessive mechanical stresses in the mid-membranous VF and disrupt the basement membrane, which is located beneath the epithelial cells and protects the lamina propria against internal stresses.^{10,11} It has been proposed that excessive collision stress is likely responsible for VF damage because it is applied directly to mucosal tissue and perpendicularly to the direction of load-bearing tissue fibers.¹² Studies with canine,¹³ feline,¹⁴ and rabbit¹¹ VFs have shown that both short and long term durations of high intensity phonation damage the basement membrane and decrease its protective ability, consequently increasing injury to the mucosal layer and underlying lamina propria. The wound healing

procedure remodels the basal layers of the epithelial cells and results in localized thickening of the epithelium and/or lamina propria.¹⁵ Over time, these areas can become stiffer and fibrosed,^{16,17} leading to the formation of more well-established lesions.^{18–21}

If sufficiently large, benign VF lesions reduce the fundamental frequency of oscillation²² and impede glottal closure by producing an hourglass-shaped glottis.^{1,23,24} This can reduce the aerodynamic energy that is transferred to the VF tissue,²⁵ thus increasing phonation threshold pressures (PTPs)^{26,27} and minimum flow rates,²⁸ as well as altering the unsteady glottal aerodynamics²⁹ and producing asymmetric aerodynamic pressure loading within the glottis.³⁰ The combination of aerodynamic and structural disruptions can significantly alter vibration mechanics, potentially resulting in asymmetric and chaotic VF oscillations^{15,31–33} that can manifest as breathy, hoarse, and/or rough voices.^{34,35}

VF nodules give rise to a slight increase in mass due to localized swelling while also increasing the tissue stiffness, which becomes more pronounced as the lesion becomes fibrosed over time.¹⁶ These rheological alterations to the VF tissue have been shown to influence the oscillation kinematics and collision dynamics.³² Of particular interest is the

^{a)}Electronic mail: berath@clarkson.edu

influence of nodules during VF collision as it is the mechanical stresses within the tissue that lead to continued lesion growth. It has been proposed that lesion growth increases the total mass of the VF,³⁶ which may subsequently lead to increased damage during collision. However, the increase in mass due to a lesion, relative to the total mass of the vibrating VF tissue, is small. Conversely, the well-established “hourglass” glottal shape, which arises with increasing nodule size,¹⁵ suggests that changes in the collision mechanics may arise due to the kinetic energy being distributed over a reduced collision area. Increased stiffness of the nodule would similarly reduce the collision time leading to a higher magnitude in the collision pressure. Despite these observations the contribution of nodule size and stiffness to VF collision mechanics remains unexplored.

This shortcoming exists, in part, because measurements of VF collision forces are extremely challenging to acquire. *In vivo* measures suffer due to the difficulty of accurately positioning a sensor in the collision zone and the resulting disruption of the airflow and VF dynamics due to physical sensor intrusion.^{37–40} Nevertheless, recent advancements using novel sensors^{39,41} and image processing techniques⁴² show significant promise. However, these methods have not yet been applied to measuring collision forces in subjects with VF nodules. Numerical studies have shown that the magnitude of the normal and shear stresses is highest at the center of the VF’s medial edge, where nodules are most prevalent⁴³ and that the physical presence of a nodule also leads to increased mechanical stresses at the base of the lesion.⁴⁴ This can lead to new acute damage or continued chronic injury and create a vicious cycle of phonotrauma.⁶ Nevertheless, prior numerical investigations have been limited to determining how lesions with fixed size and stiffness impact the oscillatory response,^{32,44,45} as opposed to exploring how these variables impact the collision mechanics. Synthetic self-oscillating silicone VF models have also explored the influence of lesions by incorporating a region of localized tissue stiffness at the center of the medial surface,^{46–48} showing that PTF and phonation threshold mean flow rate (PTF) increase significantly in VFs with nodules. However, the collision mechanics were not explored.

Consequently, it remains unclear how the progression of nodule size and stiffness alters the VF collision

mechanics. This insight is critical for understanding the role of nodule progression in phonotraumatic VF damage. The objective of this work is to investigate the influence of the size and stiffness of a representative VF lesion on VF collision mechanics using a test facility that enables exploring cases with different nodule features in a controlled environment. That is, this study explores whether the presence and progressive development (increasing size and stiffness) of a simulated nodule results in increased collision pressure, which could in turn contribute to increasing tissue trauma. Because these temporally varying behaviors are difficult, if not impossible, to assess clinically, a physical modeling approach is implemented. These results will provide useful insights for improving the prevention and diagnosis of phonotraumatic vocal hyperfunction.

II. METHODS

A. Flow facility

Investigations were performed with synthetic VF models in a hemilaryngeal flow facility, which was similar to that used in prior work.^{49–51} A schematic of the experimental setup is shown in Fig. 1. Compressed air was regulated to 17 kPa by a Siemens 40–2 pressure regulator (Siemens, Munich, Germany) before entering a Dwyer RMC 101-SSV flow meter (Dwyer Instruments, Michigan City, IN), which adjusted the subglottal pressure and measured the mean flow rate. The air flow then exited to a plenum chamber with a volume of 0.03 m³ and a cross-sectional area of 0.06 m². A 20 mm thick foam sheet was attached to the inner walls of the plenum chamber to minimize acoustic reflections. Upon exiting the plenum chamber the flow entered a 150.0 mm long rectangular channel representing the trachea with a cross-sectional area of 213.0 mm². A Kulite ET-3DC pressure transducer (Kulite Semiconductor Products, Leonia, NJ) was flush-mounted in the channel wall 30.0 mm from the exit to measure the unsteady subglottal pressure. A bracket was mounted at the exit of the tracheal channel that housed the synthetic VF model. The geometry and material properties of the synthetic VF model are discussed in Sec. II B. The lateral, anterior, and posterior surfaces of the synthetic VF model were secured to the bracket using Smooth-On Sil-poxy (Smooth-On Inc., Macungie, PA).

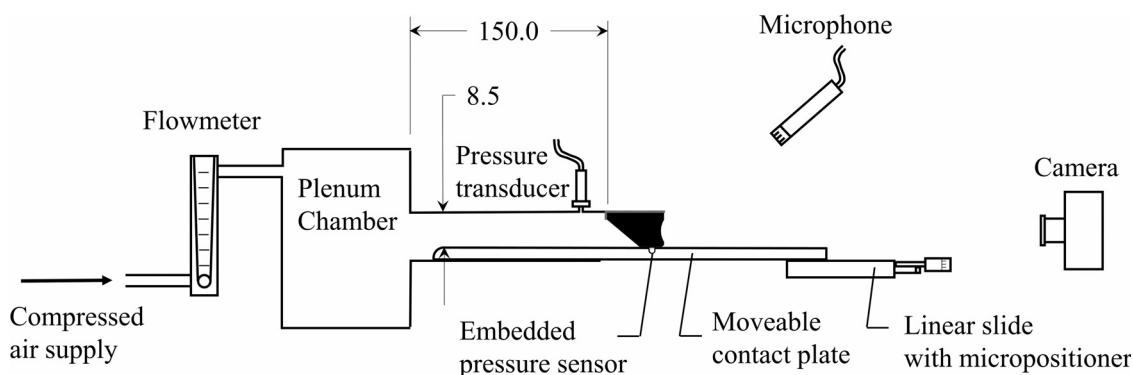


FIG. 1. Schematic of the experimental flow facility. All dimensions are in mm.

The hemilaryngeal VF oscillated against a flat plate that was 3D printed with polylactic acid. No vocal tract was included in this study.

A Millar Mikro-Cath pressure transducer (Millar, Houston, TX) embedded in the hemilaryngeal plate measured the unsteady intraglottal pressure during VF oscillation (see Motie-Shirazi *et al.*⁴⁹ for details). The sensing area of the transducer measured 1.5 mm (anterior-posterior) by 1.3 mm (inferior-superior). In this manner, the pressure sensor measured the normal impact stresses during the collision phase of VF oscillations and the aerodynamic pressure during the non-collision phase. Details of the measurement technique, calibration, and validation are provided in prior work.⁴⁹ The hemilaryngeal plate was superiorly connected to a linear slide with a micropositioner that enabled movement of the hemilaryngeal plate and, hence, the pressure transducer in the inferior-superior direction with a spatial resolution of 0.0254 mm.

The acoustic pressure was recorded with a B&K 4189 microphone (Brüel & Kjær, Nærum, Denmark) located 15.0 cm from the VF model exit and oriented at 45°. VF oscillations were recorded using a Photron AX200 high-speed camera (Photron, Tokyo, Japan) with an Elicar V-HQ Macro 90 mm f 2.5 lens (Jaca Corp., Tokyo, Japan). The camera was positioned 300.0 mm superior to the VF model and recorded at 20 000 frames per second with a spatial resolution of 0.052 mm/pixel. The subglottal, collision, and acoustic pressure data were acquired with a National Instruments PCIe-6321 data acquisition card (National Instruments Corp., Austin, TX) using a custom LabVIEW program at a sampling rate of 80 kHz for a duration of 0.75 s. The recorded high-speed video was synchronized with the pressure data measurements by generating a custom trigger signal in LabVIEW.

B. Vocal fold model

The VF model was fabricated using four layers of silicone rubber:^{52,53} namely, a base layer of adipose tissue⁵⁴ that supported the body, cover, and epithelium layers. The geometry and dimensions of these layers can be found in prior work, as well as demonstration of the ability of this

model to produce physiologically relevant oscillations.^{49–51,55} The accuracy of the intraglottal aerodynamic and collision pressure measurements obtained with this VF model has also been previously verified by comparing with prior measurements in excised VFs and static VF models.^{50,51}

A geometric protuberance representative of a VF nodule was modeled by adding a spherical bead between the cover and the epithelium layers during the fabrication process. During VF model fabrication the cover layer was cast using a mold that produced a hemispherical cavity in the medial surface with the same diameter as the bead and with a depth equal to the radius of the bead. The cavity was positioned at the anterior-posterior and inferior-superior midlines of the medial surface. The desired spherical bead was then placed in the cavity and a layer of silicone representative of the epithelial layer was added such that the bead was embedded and fixed in the VF model.¹⁵ The hemilaryngeal orientation is representative of bilateral VF nodules due to the plane of symmetry produced by the hemilaryngeal surface. A schematic showing a coronal cross section of the VF geometry is displayed in Fig. 2(a). A photograph of the corresponding physical model is shown in Fig. 2(b). The model had an anterior-posterior length of 17.0 mm.

The varying stiffness of each layer was produced by using different mixtures of Smooth-On silicone rubber and thinner (Smooth-On Inc.). The moduli of elasticity of the VF layers were measured using dynamic mechanical analysis on a TA Instruments Q 800 (TA Instruments, New Castle, DE) at a frequency of 1 Hz and 5% strain. Table I presents the VF layer, silicone type, and mixture ratio; the corresponding density and modulus of elasticity; and the physiological modulus range for the analogous human VF tissue reported in the literature. The mixture ratio of A:B:thinner in Table I denotes the ratio by weight of parts A and B of Smooth-On Ecoflex 0030 (EF) or Dragon Skin 10 (DS) silicone to thinner.

Nodules of varying diameter and stiffness were created by first fabricating spherical molds using Smooth-Sil 950 silicone (Smooth-On Inc.). Diameters of $D = 1.6, 2.0, 2.4,$ and 3.0 mm were selected based on physiological

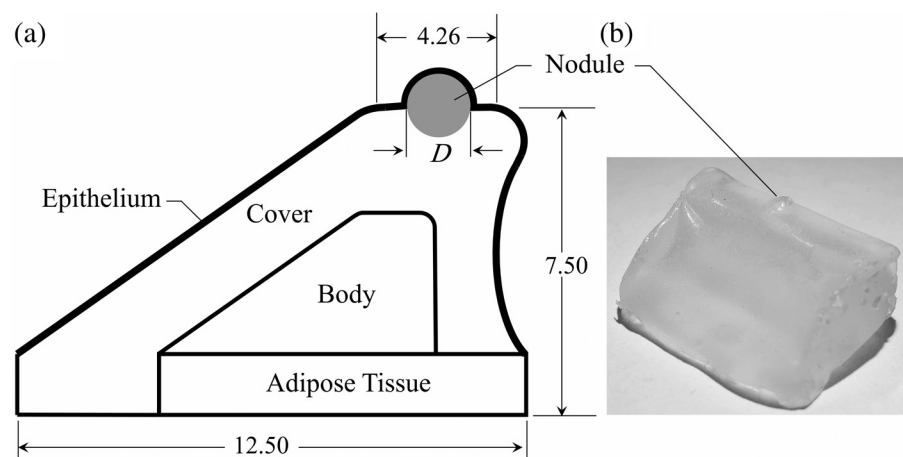


FIG. 2. (a) Geometry and key dimensions of a coronal cross section of the synthetic vocal fold model with a nodule. All dimensions are in mm. (b) Photograph of a fabricated silicone vocal fold model.

TABLE I. Vocal fold layer, silicone mixture ratio, density, measured modulus of elasticity, and the corresponding range of physiological values. Smooth-On Ecoflex 0030 and Dragon Skin 10 silicone mixtures are denoted parenthetically by EF and DS, respectively.

Layer	Silicone ratio	Density (kg/m ³)	Modulus of elasticity (kPa)	Modulus of elasticity physiological range (kPa)
Adipose tissue	1:1:4 (EF)	1041.2	5.8	1–10 (Ref. 56)
Body	1:1:2 (EF)	1061.5	13.2	1.5–50 (Refs. 57–59)
Cover	1:1:8 (EF)	1026.8	1.0	1–8 (Refs. 58 and 60–64)
Epithelium	1:1:1 (DS)	1081.2	102.5	Not measured

observations that most nodules are smaller than 3 mm.²⁴ The beads were cast using either Smooth-On EF or DS silicone mixtures to produce the desired modulus of elasticity.

The physiological range of nodule elastic moduli is not well known, although nodules are typically stiffer than the surrounding VF tissue⁴⁴ and become more fibrosed over time, thus, increasing in stiffness.¹⁶ Consequently, four different moduli of elasticity were generated to mimic nodules of increasing stiffness. Three cast beads were implemented to represent moduli of elasticity of $E_{\text{nodule}} = 13.2, 54.7,$ and 102.5 kPa. The moduli of elasticity of the cast nodules were measured with the same technique introduced above. Finally, a nylon plastic sphere (Bal-Tec, Florence-Graham, CA) was also implemented, which had an elastic modulus of $E_{\text{nodule}} = 3 \times 10^6$ kPa and acted as a limiting case of nodule stiffness.

Table II presents the size, material, modulus of elasticity, and density of the nodules used in this study. The influence of nodule size was investigated using a fixed bead with $E_{\text{nodule}} = 54.7$ kPa and varying diameters of $D = 1.6, 2.0, 2.4,$ and 3.0 mm (nodules 1–4 in Table II), where $L = 17.0$ mm was the anterior-posterior length of the VF model. The effect of nodule stiffness was studied using a fixed bead diameter of $D = 2.4$ mm while varying the moduli of elasticity across four discrete values of $E_{\text{nodule}} = 13.2, 54.7, 102.5,$ and 3×10^6 kPa (nodules 3 and 5–7 in Table II). The physiological value of the nodule density has not been reported, but it can be reasonably expected to lie within

TABLE II. Size, material, modulus of elasticity, density, and percent increase in the vibrating mass of the nodules. Smooth-On Ecoflex 0030 and Dragon Skin 10 silicone mixtures are denoted parenthetically by EF and DS, respectively.

Nodule index	Diameter (mm)	Material	Modulus of elasticity (kPa)	Density (kg/m ³)	Mass increase (%)
1	1.6	1:1:2 (DS)	54.7	1074.7	0.86
2	2.0	1:1:2 (DS)	54.7	1074.7	1.68
3	2.4	1:1:2 (DS)	54.7	1074.7	2.90
4	3.0	1:1:2 (DS)	54.7	1074.7	5.67
5	2.4	1:1:2 (EF)	13.2	1061.5	2.83
6	2.4	1:1:1 (DS)	102.5	1081.2	2.94
7	2.4	Nylon plastic	3×10^6	1150.0	3.30

the range of density for human tissues, which has been reported to be $950\text{--}1100$ kg/m³.^{65,66} The percent increase in the vibrating mass due to the added mass of the nodule, which varied with size and nodule material, is presented in the last column of Table II. It has been shown that the VF vibration has the highest magnitude inside the cover layer in regions close to the medial surface of the VF.⁶⁷ Therefore, the vibrating mass was conservatively estimated as the mass of the cover layer that is located above (medially to) a plane that is coincident with the top medial surface of the body layer. This region had a width of 2.5 mm, as shown in Fig. 2. The VF tissue was fixed at the anterior/posterior ends and experienced the highest velocity at the anterior-posterior midline. Assuming a linear change in velocity amplitude from the midline to the anterior/posterior ends, the effective oscillatory mass can be estimated as one half of the total mass of this region. This results in a vibratory mass of 0.14 g in the cover layer. The largest nodule resulted in only a 5.67% increase in vibratory mass. Consequently, the role of the added vibratory mass due to the nodule was negligible.

C. Experimental procedure

A static medial prephonatory compression of 0.50 mm was applied to the VF models to ensure repeatable VF collision. This compression was defined as the distance by which the flat portion of the medial surface of the VF cover layer is deformed medially into the hemilaryngeal plate.⁴⁹

PTP, defined as the minimum subglottal pressure required for self-sustained oscillations of the VFs, was found by gradually increasing the subglottal pressure until self-sustained VF oscillations were achieved. PTP, PTF, sound pressure level at the threshold pressure (SPL_t), and fundamental frequency at the threshold pressure ($f_{o,t}$) were measured for each model. The inferior-superior location along the VF midline at which peak collision pressure occurred at PTP was identified by traversing the collision pressure sensor in the inferior-superior direction. Once the location of peak pressure was determined the time-varying pressure waveform was acquired at that position over the 0.75 s data acquisition time (approximately 130 cycles). The pressure waveforms were then segmented and phase-averaged according to the oscillation period. As an example, Fig. 3 shows the temporal evolution of two successive cycles of intraglottal pressure, p_{int} , for a VF with a nodule of size $D = 3.0$ mm and stiffness $E_{\text{nodule}} = 54.7$ kPa at the PTP of 4.22 kPa. The time intervals of the different phases of VF oscillation were extracted based on the synchronized high-speed video and are labeled in Fig. 3. The high-speed video can be found in the supplementary materials as SuppPub1.mp4.⁶⁸ The intraglottal pressure signal exhibits a sharp peak during the collision phase (T_c) followed by a second peak that is lower in magnitude and that corresponds to the increase in the aerodynamic pressure as the pressure sensor is exposed to the subglottal pressure during the glottal opening phase (T^+). The pressure then decreases during the closing phase (T^-) due to flow acceleration through the

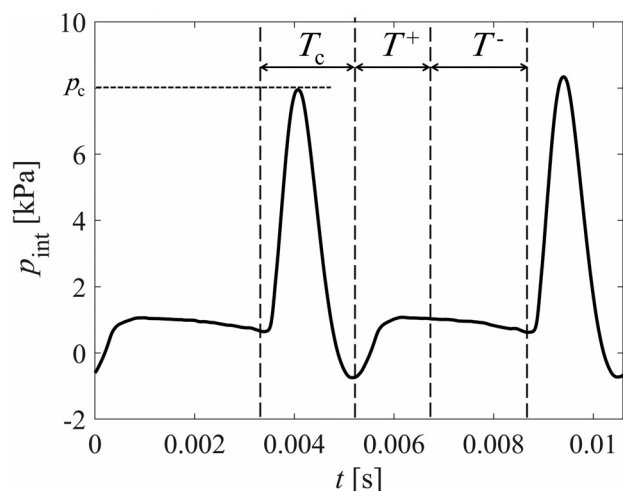


FIG. 3. Two successive cycles of the intraglottal pressure waveform measured at the PTP (of 4.22 kPa for a vocal fold with a nodule of size $D = 3.0$ mm and nodule modulus of $E_{\text{nodule}} = 54.7$ kPa). Three phases of the oscillation cycle are indicated: collision phase (T_c), glottal opening phase (T^+), and glottal closing phase (T^-).

glottis. During the VF collision phase the maximum pressure magnitude corresponds to the peak collision pressure, p_c . This measure served as an indicator to quantitatively compare the potential risk of further VF damage as a function of nodule size and stiffness.

The peak collision pressure was obtained only at the phonation threshold condition because increasing the subglottal pressure to a value significantly higher than the PTP resulted in irregular, aperiodic VF oscillations. When this occurred, the location and magnitude of the VF collision changed significantly from cycle to cycle and repeatable measurements could not be achieved. Numerical investigations have similarly shown that adding a mass to the VFs produces chaotic vibrations at high subglottal pressures.³²

The sound pressure level (SPL) normalized by aerodynamic power, denoted as P' , was calculated as the ratio of SPL at PTP (SPL_t) to the logarithmically scaled product of PTP and PTF, such that $P' = \text{SPL}_t / [10 \log(\text{PTP} \cdot \text{PTF})]$. Clinical studies have shown that this measure can reliably differentiate patients with VF lesions from healthy groups.^{69,70}

III. RESULTS

A. Effect of nodule size

The PTP and PTF of the VF model without a nodule were measured to be 1.75 kPa and 298 ml/s, respectively. These values were higher than the expected physiological range for PTP in healthy human phonation⁷¹ due to the hemilaryngeal configuration, which is known to increase PTP.^{41,72,73} Applying prephonatory compression, which was required to achieve robust collision during VF oscillation, also increases PTP.⁷⁴ Nevertheless, the VF model exhibited a fundamental frequency of $f_{o,t} = 189$ Hz and maximum glottal hemilaryngeal width of 0.86 mm, which are physiologically representative values.^{75,76} In addition, the open quotient was 0.70, and the speed quotient was 0.97, which

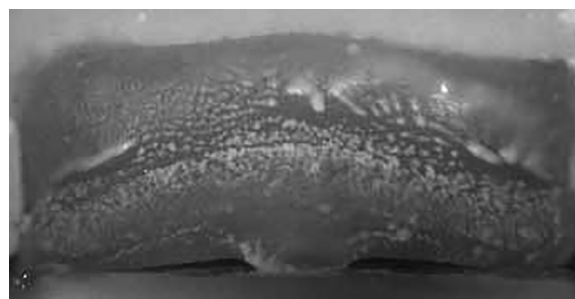


FIG. 4. Superior view of the hourglass-shaped glottis at minimal glottal area for the vocal fold with a nodule size of $D = 3$ mm and nodule modulus of $E_{\text{nodule}} = 54.7$ kPa.

were within the range of physiological values.^{77,78} Furthermore, prior studies^{50,51} have shown that despite having higher than normal subglottal pressure of the VF models, normalizing the collision and intraglottal aerodynamic pressures by the mean subglottal pressure results in very good agreement with the values and behaviors reported with excised VFs⁷² and static VF models.⁷⁹ The SPL at phonation threshold, SPL_t , was 70 dB, measured at a distance of 15.0 cm from the glottal exit. High-speed video of oscillations for the VF without a nodule can be found in the supplementary materials as SuppPub2.mp4.⁶⁸

Adding a nodule to the VF model resulted in one side of the typical hourglass-shaped glottal closure during oscillations, which is commonly observed *in vivo*.^{23,80} This hourglass closure was more pronounced in models with larger nodule sizes. See supplementary files SuppPub3.mp4, SuppPub4.mp4, and SuppPub5.mp4 for the high-speed videos of the VFs with nodule size of 1.6, 2.0, and 2.4 mm, respectively.⁶⁸ Figure 4 displays an extracted image from the high-speed video showing the resulting hourglass shape when the glottal area was a minimum for the VF model with the largest nodule ($D = 3.0$ mm). For this VF model the glottal width at the mid-anterior-posterior distance ($w_{\text{gt,mid}}$) where the nodule is located and the glottal area (A_{gt}) are plotted as functions of time in Fig. 5. The glottal area was

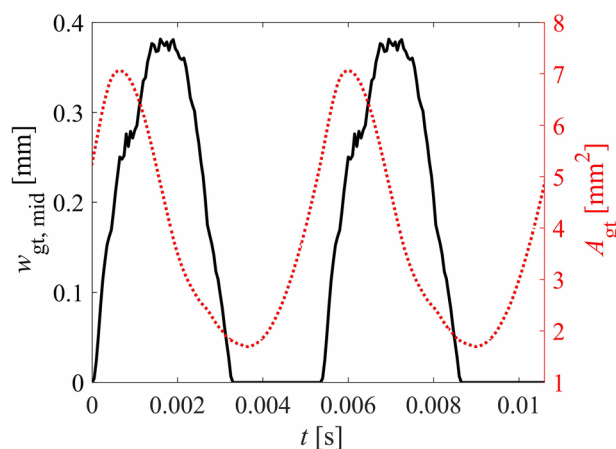


FIG. 5. (Color online) Time series of the glottal width at the mid-anterior-posterior distance $w_{\text{gt,mid}}$ (solid line, left axis) and the glottal area A_{gt} (dotted line, right axis) for the vocal fold with a nodule size of $D = 3$ mm and nodule modulus of $E_{\text{nodule}} = 54.7$ kPa.

always greater than zero, indicating that the VF never experienced complete closure during oscillation.

Figure 6 presents aerodynamic and acoustic measures as a function of nodule diameter with a constant nodule elastic modulus of 54.7 kPa. Note that each data point in the plots presented in this article refers to the value measured using a single VF model. The error bars indicate the cumulative error of the tolerance of the measuring instrument and the variation in the measured parameter over the recorded VF oscillation cycles. Figure 6(a) shows that increasing nodule size resulted in a monotonic increase in PTP, which is in agreement with prior clinical investigations reporting higher PTPs in patients with VF lesions.²⁶ The PTP for the largest

nodule ($D = 3$ mm) was 140% higher than that of the VF model without a nodule ($D = 0$ mm). The increase in PTP with nodule diameter resulted in similarly increasing PTFs and SPLs, as shown in Figs. 6(b) and 6(c), respectively, which is also consistent with trends observed in clinical measurements.^{26,28} For the largest nodule size, the PTF and SPL were 121% and 13.5 dB higher than corresponding values for the VF without a nodule, respectively. The fundamental frequency of oscillation at PTP, however, showed a minor decrease in about 7 Hz, as shown in Fig. 6(d).

Figure 6(e) presents the open quotient as a function of nodule diameter. As the nodule diameter increased, the duration of glottal closure decreased, resulting in higher

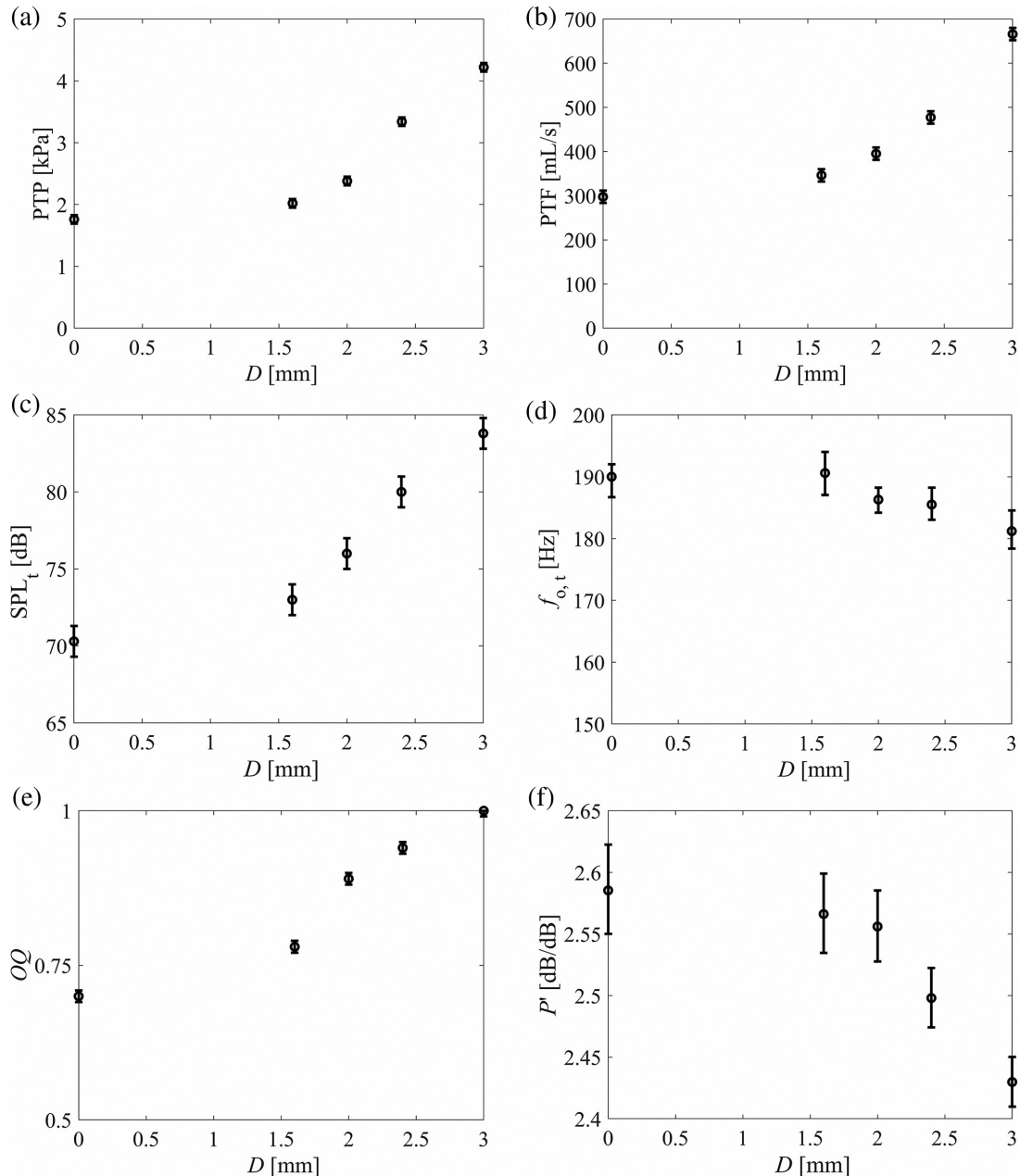


FIG. 6. Values of (a) PTP, (b) PTF, (c) SPL, (d) fundamental frequency, (e) open quotient, and (f) SPL normalized by aerodynamic power as a function of nodule diameter for $E_{\text{nodule}} = 54.7$ kPa. The markers denote the mean value, and the error bars indicate the maximum and minimum values recorded over the 0.75 s acquisition time. $D = 0$ mm represents the experimental condition with no simulated nodule present.

open quotient values, which is also in agreement with clinical investigations.⁸¹ The open quotient for the largest nodule ($D = 3$ mm) was 1, indicating that a glottal gap was always present, as shown in Fig. 4. The influence of the nodule size on the SPL normalized by the aerodynamic power, P' , is shown in Fig. 6(f), where the values decreased by 6% with increasing nodule diameter.

The ratio of the peak collision pressure to the PTP, p_c/PTP , as a function of nodule diameter is presented in Fig. 7. An increase in p_c/PTP was observed with increasing nodule diameter, starting at 0.7, when no nodule was present, and remaining largely unchanged for the VF with a nodule size of $D = 1.6$ mm. However, when the nodule size increased to $D = 3$ mm, the pressure ratio increased dramatically to a value of 2. This was an increase of 186% relative to the case without a nodule.

B. Effect of nodule stiffness

The influence of nodule stiffness was investigated by varying the modulus of elasticity for a constant nodule diameter of $D = 2.4$ mm, as described in Sec. II C. High-speed videos of the VF oscillations for nodule stiffnesses of 13.2, 54.7, 102.5, and 3×10^6 kPa can be found in the supplementary materials as SuppPub6.mp4, SuppPub5.mp4, SuppPub7.mp4, and SuppPub8.mp4, respectively.⁶⁸ Figures 8(a)–8(e) present the PTP, PTF, $SPL_{t,f_{o,t}}$, and P' as a function of the nodule modulus of elasticity. The investigated moduli of elasticity were $E_1 = 13.2$ kPa, $E_2 = 54.7$ kPa, $E_3 = 102.5$ kPa, and $E_4 = 3 \times 10^6$ kPa. These parameters changed by less than 8% over the broad range of elastic moduli, indicating that nodule stiffness does not substantially influence the aerodynamic, kinematic, and acoustic parameters. In contrast, a significant increase in the peak collision pressure as a function of increasing nodule stiffness is observed in Fig. 8(f), with p_c/PTP for the stiffest nodule being nearly 400% higher than that for the softest nodule.

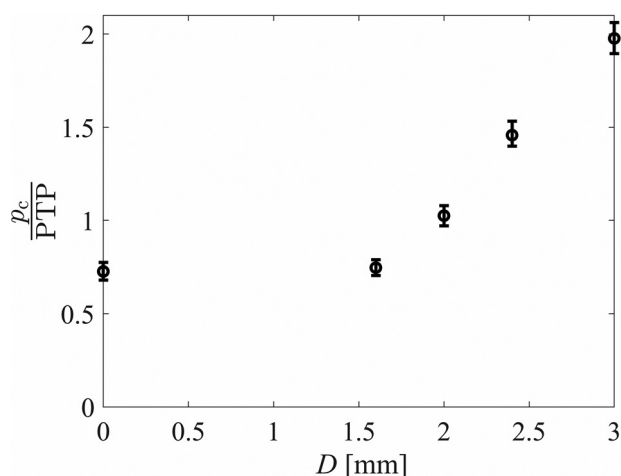


FIG. 7. The ratio of the collision pressure to the PTP as a function of nodule diameter for the case of $E_{\text{nodule}} = 54.7$ kPa. The markers denote the mean value, and the error bars indicate the maximum and minimum values.

The influence of nodule stiffness on collision mechanics can be further explored by investigating the intraglottal pressure waveform of the VFs as a function of nodule stiffness. Figure 9 shows the ratio of VF intraglottal pressure to the PTP (p_{int}/PTP) as a function of time for the four nodule stiffnesses. The intraglottal pressures were synchronized based on the simultaneously recorded subglottal pressure waveform and were phase-averaged over 130 oscillation cycles. As shown in Fig. 9, as nodule stiffness increases, the time of contact decreases, and the magnitude of the collision pressure increases accordingly.

IV. DISCUSSION

The emergence and growth of VF nodules has commonly been attributed to excessive mechanical stresses applied to the VF tissue.^{12,18,19,21} Nodules become larger and stiffer over time, which can increase collision stresses and create a vicious cycle of increasing VF phonotrauma.^{5,6} This study sheds light on how the progressive development of nodules contributes to escalating phonotraumatic damage by studying the effect of nodule size and stiffness on VF collision pressure. Unlike *in vivo* investigations, the experimental framework utilized herein does not disrupt the glottal airflow and VF dynamics and has precise sensor positioning that allows high-fidelity determination of the resultant collision pressures.

Increasing nodule size led to increased PTP and PTF, which can be explained by considering the influence of nodules on the VF geometry and the resultant dynamics. As shown in Fig. 4, the presence of a nodule resulted in an hourglass-shaped glottal closure. These findings were consistent with prior work that has shown that increasing the medial prephonatory distance between the VFs (i.e., incomplete glottal closure) increases the energy required for oscillation and results in higher PTP.^{4,25,82,83} Both clinical and experimental results have similarly shown that nodules produce higher PTP and PTF.^{26–28} Consistent with this observation, nodule stiffness did not have a considerable effect on the bulk aerodynamic and VF kinematic measures.

However, the collision mechanics were profoundly influenced by nodule stiffness and size. A nodule diameter of 3.0 mm resulted in an increase in the ratio of collision pressure to subglottal pressure of 186% (see Fig. 8). This was despite the added vibratory mass, and hence the kinetic energy of the VF, increasing by $\leq 5.67\%$. Consequently, the influence of the added vibratory mass of a nodule on the collision pressure was deemed inconsequential. The increase in the ratio of collision to subglottal pressure was much higher in VF models with a nodule when compared to those without a nodule.⁴² For VFs without a nodule, increasing the subglottal pressure from 2.0 to 3.4 kPa resulted in a 26% increase in the of collision to subglottal pressure.⁴² Conversely, in VF models with a nodule, a similar increase in subglottal pressure resulted in a 96% increase in the ratio of collision to subglottal pressure. It can therefore be inferred that the increase in the collision pressure is predominantly due to the presence of a nodule rather than the

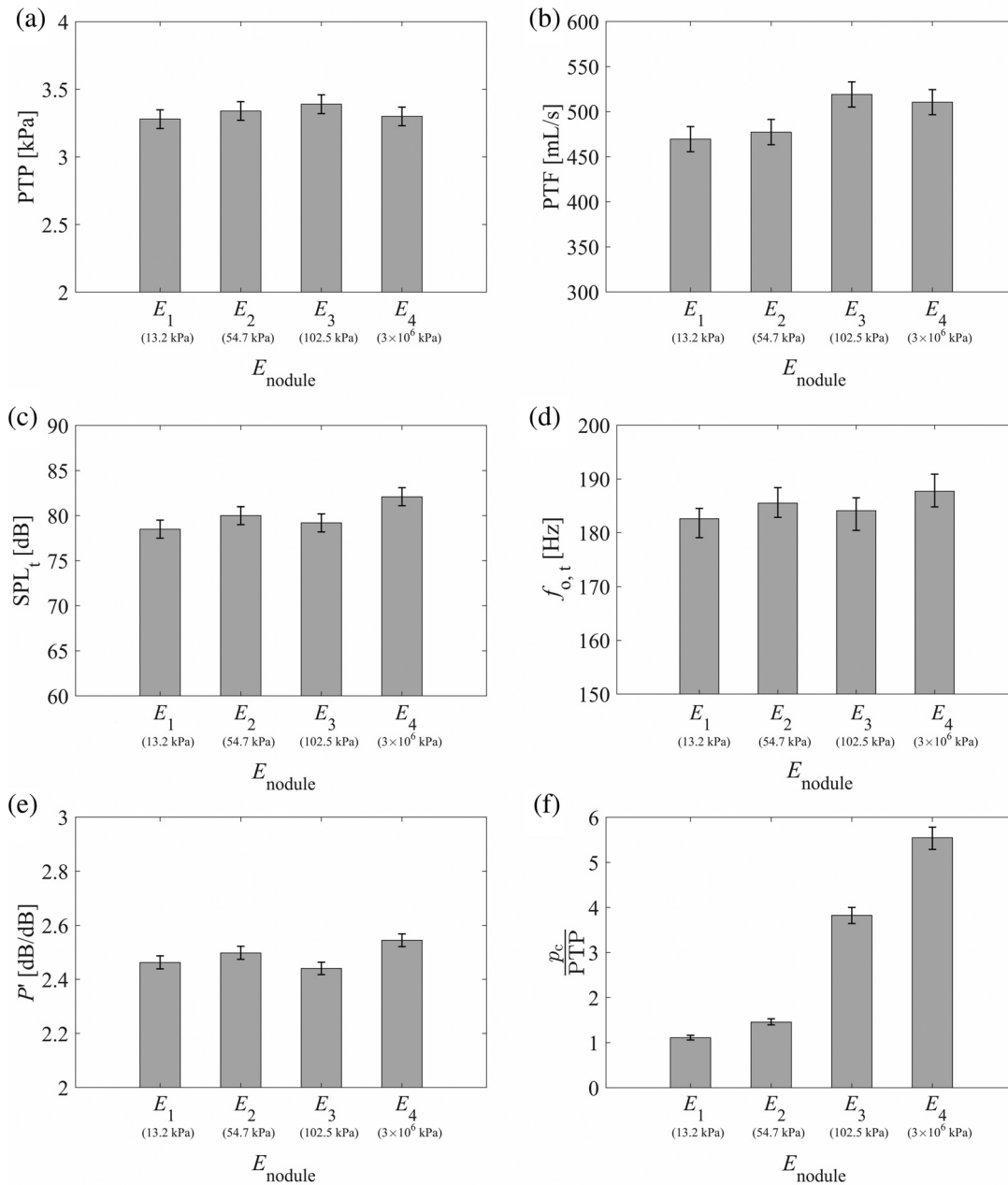


FIG. 8. Values of (a) PTP, (b) PTF, (c) SPL_{-1} , (d) $f_{o,t}$, (e) P' , and (f) ratio of collision pressure to subglottal pressure as a function of the nodule modulus of elasticity. The bars denote mean values, and the error bars indicate the maximum and minimum values.

increase in the subglottal pressure, although increasing subglottal pressure also plays a role. The implication is that as nodule size increases, the potential for further phonotrauma rises dramatically. Similarly, increasing the nodule stiffness while keeping the size constant resulted in a 400% increase in the ratio of collision to subglottal pressure despite a negligible increase of 0.5% in the vibrating mass (see Table II) and a largely constant PTP. Together, these results provide novel insights into the mechanics of VF collision, indicating that nodule size and stiffness drastically influence collision stresses.

This occurs for two reasons. First, for increasing nodule sizes, the total kinetic energy of the VF is distributed over a smaller contact area. Collision first occurs at the cap of the

nodule, creating a drastically reduced initial contact patch compared with that arising during healthy VF collision. In addition, the protruding surface of the nodule prevents the surrounding tissue from subsequently coming into contact with the opposing VF surface, as observed by the hourglass orientation during collision (see Fig. 4). As such, the contact area at the cap of the VF nodule experiences the majority of the load responsible for converting kinetic VF energy into elastic potential energy during collision. Second, as nodule stiffness increases, the nodule experiences a smaller deformation during collision, which results in a shorter time of collision (see Fig. 9), and the magnitude of the collision pressure increases accordingly.

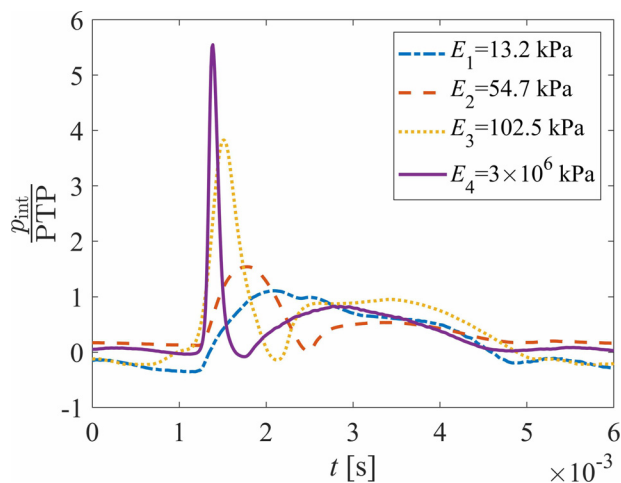


FIG. 9. (Color online) The ratio of the intraglottal pressure to the PTP as a function of time for nodules with different moduli of elasticity.

Simultaneously considering the effects of increasing nodule size and stiffness provides unique insight into the repetitive and worsening cycle of VF injury.^{5,6} Namely, as a lesion develops and produces a geometric protuberance the collision pressure and the associated tissue stress increase with nodule size. Compensatory behaviors that aim to restore SPL, such as increasing subglottal pressure, further increase the magnitude of the collision pressures.⁴ As the pathology progresses and the lesion becomes stiff and fibrosed, collision pressures are further exacerbated, and the cycle of damage is accelerated.

However, in the early stages of nodule development, only modest increases in the collision pressure occur. For example, the ratio of collision pressure to subglottal pressure does not increase considerably for a small nodule ($D = 1.6$ mm; see Fig. 7). This result supports the prevailing clinical view that early clinical diagnosis and treatment can effectively stave off the more severe consequences that may arise if left unaddressed.^{5,6} Further support for this theory is also provided by clinical studies that have shown that performing voice therapy can reduce nodule size and appears to have a trauma-reducing effect on small nodules.⁷ In agreement with these observations it was found that SPL normalized by aerodynamic power, P' , decreased with increasing nodule size, indicating increased phonatory effort. Similar results have been reported in clinical investigations where values of P' were found to effectively differentiate between individuals with VF nodules and vocally healthy controls.^{69,70}

It should be noted that the current modeling approach is based on assumptions that may influence the physiological interpretation. First, the nodules were modeled as a localized stiffness when, in reality, they have a broad base of fibrous tissue that creates a stiffness gradient inside the VF tissue.⁸⁴ Second, the nodules were placed exactly at the inferior-superior and medial-lateral midlines of the medial VF surface. Changes in the position may give rise to more asymmetrical VF oscillations, which could alter the VF dynamics. In addition, the collision pressures reported herein are measured at the

VF surface, as opposed to inside the tissue. Investigating the influence of nodules on internal VF stresses remains a subject of future work. Moreover, the VF models oscillated at a higher than normal subglottal pressure, which may influence the physics of VF oscillations and, consequently, the collision mechanics. Utilizing models with lower PTPs that more closely correspond with the physiological range would help to verify the collision pressure trends observed herein. Finally, due to the complexity of the model fabrication and pressure measurements, which required all VF models to be fabricated at the same time and then tested within a one-day window, a limited number of VF models (five nodule sizes and four moduli of elasticity) were fabricated and tested. Nevertheless, a clear and unambiguous trend of the collision pressure increasing as a function of nodule size and stiffness was demonstrated.

V. CONCLUSIONS

The effect of VF nodule size and stiffness on peak collision pressure was investigated with self-oscillating synthetic VF models in a hemilaryngeal flow facility. The presence of a simulated nodule created an hourglass closure and increased the open quotient. Increasing the nodule diameter increased the PTP, PTF, and SPL. Most importantly, despite a minor increase in the VF mass due to adding a nodule, the ratio of collision pressure to subglottal pressure increased significantly with both increasing nodule size and stiffness. These findings reinforce the hypothesis of a chronic, deleterious cycle of VF damage that arises due to phonotrauma as VF nodules increase in both size and stiffness. Encouragingly, results indicate that these damaging effects are most pronounced for relatively large, stiff nodules, supporting the prevailing clinical view that early clinical diagnosis and intervention may prevent further VF tissue damage and, in some cases, can reduce the damage that has already occurred.

ACKNOWLEDGMENTS

This research was supported by the National Institutes of Health National Institute on Deafness and Other Communication Disorders Grant No. P50 DC015446 and Agencia Nacional de Investigación y Desarrollo Grant No. BASAL FB0008. The content is solely the responsibility of the authors and does not necessarily represent the official views of the National Institutes of Health. M.Z. has a financial interest in Lanek SPA, a company focused on developing and commercializing biomedical devices and technologies. M.Z.'s interests were reviewed and are managed by Universidad Técnica Federico Santa María in accordance with its conflict-of-interest policies. R.H. and D.M. have a financial interest in InnoVoyce LLC, a company focused on developing and commercializing technologies for the prevention, diagnosis, and treatment of voice-related disorders. R.H.'s and D.M.'s interests were reviewed and are managed by Massachusetts General Hospital and Mass General Brigham in accordance with their conflict-of-interest policies.

- ¹F. G. Dikkers and P. G. Nikkels, "Benign lesions of the vocal folds: Histopathology and phonotrauma," *Ann. Otol. Rhinol. Laryngol.* **104**(9), 698–703 (1995).
- ²M. Lee, T. Mau, and L. Sulica, "Patterns of recurrence of phonotraumatic vocal fold lesions suggest distinct mechanisms of injury," *Laryngoscope* **131**, 2523–2529 (2021).
- ³D. de Vasconcelos, A. O. C. Gomes, and C. M. T. de Araújo, "Vocal fold polyps: Literature review," *Int. Arch. Otorhinolaryngol.* **23**(1), 116–124 (2019).
- ⁴G. E. Galindo, S. D. Peterson, B. D. Erath, C. Castro, R. E. Hillman, and M. Zañartu, "Modeling the pathophysiology of phonotraumatic vocal hyperfunction with a triangular glottal model of the vocal folds," *J. Speech Lang. Hear. Res.* **60**(9), 2452–2471 (2017).
- ⁵R. E. Hillman, E. B. Holmberg, J. S. Perkell, M. Walsh, and C. Vaughan, "Objective assessment of vocal hyperfunction: An experimental framework and initial results," *J. Speech Hear. Res.* **32**, 373–392 (1989).
- ⁶R. E. Hillman, C. E. Stepp, J. H. Van Stan, M. Zañartu, and D. D. Mehta, "An updated theoretical framework for vocal hyperfunction," *Am. J. Speech Lang. Pathol.* **29**(4), 2254–2260 (2020).
- ⁷E. B. Holmberg, R. E. Hillman, B. Hammarberg, M. Södersten, and P. Doyle, "Efficacy of a behaviorally based voice therapy protocol for vocal nodules," *J. Voice* **15**(3), 395–412 (2001).
- ⁸J. Kuo, E. B. Holmberg, and R. E. Hillman, "Discriminating speakers with vocal nodules using aerodynamic and acoustic features," in *Proceedings of the 1999 IEEE International Conference on Acoustics, Speech, and Signal Processing (ICASSP99) (Cat. No.99CH36258)*, Phoenix, AZ (March 15–19, 1999), pp. 77–80.
- ⁹C. E. Stepp, R. E. Hillman, and J. T. Heaton, "A virtual trajectory model predicts differences in vocal fold kinematics in individuals with vocal hyperfunction," *J. Acoust. Soc. Am.* **127**(5), 3166–3176 (2010).
- ¹⁰E. E. Levendoski, C. Leydon, and S. L. Thibeault, "Vocal fold epithelial barrier in health and injury: A research review," *J. Speech Lang. Hear. Res.* **57**(5), 1679–1691 (2014).
- ¹¹B. Rousseau, A. Suehiro, N. Echemendia, and M. Sivasankar, "Raised intensity phonation compromises vocal fold epithelial barrier integrity," *Laryngoscope* **121**(2), 346–351 (2011).
- ¹²I. R. Titze, "Mechanical stress in phonation," *J. Voice* **8**(2), 99–105 (1994).
- ¹³S. Gray and I. Titze, "Histologic investigation of hyperphonated canine vocal cords," *Ann. Otol. Rhinol. Laryngol.* **97**, 381–388 (1988).
- ¹⁴R. Zhao, Y. Cai, and H. Wang, "Pathological changes of hyperphonated cat vocal folds," *Auris Nasus Larynx* **18**(1), 55–59 (1991).
- ¹⁵M. M. Johns, "Update on the etiology, diagnosis, and treatment of vocal fold nodules, polyps, and cysts," *Curr. Opin. Otolaryngol. Head Neck Surg.* **11**, 456–461 (2003).
- ¹⁶R. C. Branski, K. Verdolini, V. Sandulache, C. A. Rosen, and P. A. Hebda, "Vocal fold wound healing: A review for clinicians," *J. Voice* **20**(3), 432–442 (2006).
- ¹⁷R. Mittal, B. D. Erath, and M. W. Plesniak, "Fluid dynamics of human phonation and speech," *Annu. Rev. Fluid Mech.* **45**, 437–467 (2013).
- ¹⁸M. S. Courey, M. A. Scott, J. A. Shohet, and R. H. Ossoff, "Immunohistochemical characterization of benign laryngeal lesions," *Ann. Otol. Rhinol. Laryngol.* **105**(7), 525–531 (1996).
- ¹⁹F. G. Dikkers and P. G. Nikkels, "Lamina propria of the mucosa of benign lesions of the vocal folds," *Laryngoscope* **109**(10), 1684–1689 (1999).
- ²⁰S. D. Gray, E. Hammond, and D. F. Hanson, "Benign pathologic responses of the larynx," *Ann. Otol. Rhinol. Laryngol.* **104**(1), 13–18 (1995).
- ²¹S. Hirano, D. M. Bless, B. Rousseau, N. Welham, T. Scheidt, and C. N. Ford, "Fibronectin and adhesion molecules on canine scarred vocal folds," *Laryngoscope* **113**, 966–972 (2003).
- ²²R. Greiss, J. Rocha, and E. Matida, "Modal analysis of a parameterized model of pathological vocal fold vibration," in *Proceedings of the 2016 IEEE EMBS International Student Conference (ISC)*, Ottawa, Canada (May 29–31, 2016).
- ²³P. H. Dejonckere and M. Kob, "Pathogenesis of vocal fold nodules: New insights from a modelling approach," *Folia Phoniatr. Logop.* **61**(3), 171–179 (2009).
- ²⁴L. Wallis, C. Jackson-Menaldi, W. Holland, and A. Giraldo, "Vocal fold nodule vs. vocal fold polyp: Answer from surgical pathologist and voice pathologist point of view," *J. Voice* **18**, 125–129 (2004).
- ²⁵I. R. Titze, "The physics of small-amplitude oscillation of the vocal folds," *J. Acoust. Soc. Am.* **83**(4), 1536–1552 (1988).
- ²⁶J. Jiang, T. O'Mara, D. Conley, and D. Hanson, "Phonation threshold pressure measurements during phonation by airflow interruption," *Laryngoscope* **109**, 425–432 (1999).
- ²⁷S. Deguchi and Y. Kawahara, "Simulation of human phonation with vocal nodules," *Am. J. Comput. Math.* **1**(3), 189–201 (2011).
- ²⁸P. Zhuang, A. J. Sprecher, M. R. Hoffman, Y. Zhang, M. Fourakis, J. J. Jiang, and C. S. Wei, "Phonation threshold flow measurements in normal and pathological phonation," *Laryngoscope* **119**(4), 811–815 (2009).
- ²⁹B. D. Erath and M. W. Plesniak, "Three-dimensional laryngeal flow fields induced by a model vocal fold polyp," *Int. J. Heat Fluid Flow* **35**, 93–101 (2012).
- ³⁰L. R. Ranjbar, "Experimental and computational study of intraglottal pressure distributions for vocal polyps," Ph.D. thesis, University of Toledo, Toledo, OH, 2018.
- ³¹A. Yamauchi, H. Yokonishi, H. Imagawa, K. Sakakibara, T. Nito, N. Tayama, and T. Yamasoba, "Quantification of vocal fold vibration in various laryngeal disorders using high-speed digital imaging," *J. Voice* **30**(2), 205–214 (2016).
- ³²Y. Zhang and J. J. Jiang, "Chaotic vibrations of a vocal fold model with a unilateral polyp," *J. Acoust. Soc. Am.* **115**(3), 1266–1269 (2004).
- ³³Y. Zhang and J. J. Jiang, "Asymmetric spatiotemporal chaos induced by a polypoid mass in the excised larynx," *Chaos Interdiscip. J. Nonlinear Sci.* **18**(4), 043102 (2008).
- ³⁴J. K. Kutty and K. Webb, "Tissue engineering therapies for the vocal fold lamina propria," *Tissue Eng. Part B Rev.* **15**(3), 249–262 (2009).
- ³⁵I. R. Titze, *Principles of Voice Production* (Prentice-Hall, Englewood Cliffs, NJ, 1994).
- ³⁶M. Civera, C. Filosi, N. Pugno, M. Silvestrini, C. Surace, and K. Worden, "Assessment of vocal cord nodules: A case study in speech processing by using Hilbert-Huang transform," *J. Phys. Conf. Ser.* **842**, 012025 (2017).
- ³⁷H. E. Gunter, R. D. Howe, S. M. Zeitels, J. B. Kobler, and R. E. Hillman, "Measurement of vocal fold collision forces during phonation," *J. Speech Lang. Hear. Res.* **48**(3), 576–576 (2005).
- ³⁸M. M. Hess, K. Verdolini, W. Bierhals, U. Mansmann, and M. Gross, "Endolaryngeal contact pressures," *J. Voice* **12**, 50–67 (1998).
- ³⁹D. D. Mehta, J. B. Kobler, S. M. Zeitels, M. Zañartu, E. J. Ibarra, G. A. Alzamendi, R. Manriquez, B. D. Erath, S. D. Peterson, R. H. Petrillo, and Hillman, R. E., "Direct measurement and modeling of intraglottal, subglottal, and vocal fold collision pressures during phonation in an individual with a hemilaryngectomy," *Appl. Sci.* **11**(16), 7256 (2021).
- ⁴⁰K. Verdolini, M. M. Hess, I. R. Titze, W. Bierhals, and M. Gross, "Investigation of vocal fold impact stress in human subjects," *J. Voice* **13**(2), 184–202 (1999).
- ⁴¹D. D. Mehta, J. B. Kobler, S. M. Zeitels, M. Zañartu, B. D. Erath, M. Motie-Shirazi, S. D. Peterson, R. H. Petrillo, and R. E. Hillman, "Toward development of a vocal fold contact pressure probe: Bench-top validation of a dual-sensor probe using excised human larynx models," *Appl. Sci.* **9**(20), 4360 (2019).
- ⁴²M. E. Díaz-Cádiz, S. D. Peterson, G. E. Galindo, V. M. Espinoza, M. Motie-Shirazi, B. D. Erath, and M. Zañartu, "Estimating vocal fold contact pressure from raw laryngeal high-speed videendoscopy using a hertz contact model," *Appl. Sci.* **9**(11), 2384 (2019).
- ⁴³H. Gunter, "Modeling mechanical stresses as a factor in the etiology of benign vocal fold lesions," *J. Biomech.* **37**, 1119–1124 (2004).
- ⁴⁴J. J. Jiang, C. E. Diaz, and D. G. Hanson, "Finite element modeling of vocal fold vibration in normal phonation and hyperfunctional dysphonia: Implications for the pathogenesis of vocal nodules," *Ann. Otol. Rhinol. Laryngol.* **107**, 603–610 (1998).
- ⁴⁵O. Guasch, A. Van Hirtum, A. I. Fernández, and M. Arnela, "Controlling chaotic oscillations in a symmetric two-mass model of the vocal folds," *Chaos Solitons Fractals* **159**, 112188 (2022).
- ⁴⁶R. N. Rauma, "The effect of simulated nodules on vocal fold movement in a two layer synthetic model," Master's thesis, Brigham Young University-Provo, Provo, UT, 2009.
- ⁴⁷P. Luizard and X. Pelorson, "Threshold of oscillation of a vocal fold replica with unilateral surface growths," *J. Acoust. Soc. Am.* **141**(5), 3050–3058 (2017).
- ⁴⁸A. Conte, M. Maselli, A. Nacci, M. Manti, J. Galli, G. Paludetti, F. Ursino, C. Laschi, and M. Cianchetti, "Conductive silicone vocal folds

- reproducing electroglottographic signal in pathophysiological conditions," *IEEE Trans. Med. Rob. Bionics* **3**, 337–348 (2021).
- ⁴⁹M. Motie-Shirazi, M. Zaňartu, S. D. Peterson, D. D. Mehta, J. B. Kobler, R. E. Hillman, and B. D. Erath, "Toward development of a vocal fold contact pressure probe: Sensor characterization and validation using synthetic vocal fold models," *Appl. Sci.* **9**(15), 3002 (2019).
- ⁵⁰M. Motie-Shirazi, M. Zaňartu, S. D. Peterson, and B. D. Erath, "Vocal fold dynamics in a synthetic self-oscillating model: Intraglottal aerodynamic pressure and energy," *J. Acoust. Soc. Am.* **150**(2), 1332–1345 (2021).
- ⁵¹M. Motie-Shirazi, M. Zaňartu, S. D. Peterson, and B. D. Erath, "Vocal fold dynamics in a synthetic self-oscillating model: Contact pressure and dissipated-energy dose," *J. Acoust. Soc. Am.* **150**(1), 478–489 (2021).
- ⁵²P. R. Murray and S. L. Thomson, "Synthetic, multi-layer, self-oscillating vocal fold model fabrication," *J. Vis. Exp.* **58**, e3498 (2011).
- ⁵³B. A. Pickup and S. L. Thomson, "Influence of asymmetric stiffness on the structural and aerodynamic response of synthetic vocal fold models," *J. Biomech.* **42**, 2219–2225 (2009).
- ⁵⁴C. L. Jones, A. Achuthan, and B. D. Erath, "Modal response of a computational vocal fold model with a substrate layer of adipose tissue," *J. Acoust. Soc. Am.* **137**(2), EL158–EL164 (2015).
- ⁵⁵M. Motie-Shirazi, M. Zaňartu, S. D. Peterson, D. D. Mehta, R. E. Hillman, and B. D. Erath, "Collision pressure and dissipated power dose in a self-oscillating silicone vocal fold model with a posterior glottal opening," *J. Speech Lang. Hear. Res.* **65**(8), 2829–2845 (2022).
- ⁵⁶K. Comley and N. Fleck, "The compressive response of porcine adipose tissue from low to high strain rate," *Int. J. Impact Eng.* **46**, 1–10 (2012).
- ⁵⁷Y. B. Min, I. R. Titze, and F. Alipour-Haghighi, "Stress-strain response of the human vocal ligament," *Ann. Otol. Rhinol. Laryngol.* **104**(7), 563–569 (1995).
- ⁵⁸D. K. Chhetri, Z. Zhang, and J. Neubauer, "Measurement of Young's modulus of vocal folds by indentation," *J. Voice* **25**, 1–7 (2011).
- ⁵⁹G. R. Dion, P. G. Coelho, S. Teng, M. N. Janal, M. R. Amin, and R. C. Branski, "Dynamic nanomechanical analysis of the vocal fold structure in excised larynges," *Laryngoscope* **127**(7), E225–E230 (2017).
- ⁶⁰F. Alipour and S. Vigmostad, "Measurement of vocal folds elastic properties for continuum modeling," *J. Voice* **26**(6), 816.E21–816.E29 (2012).
- ⁶¹R. W. Chan and I. R. Titze, "Viscoelastic shear properties of human vocal fold mucosa: Measurement methodology and empirical results," *J. Acoust. Soc. Am.* **106**, 2008–2021 (1999).
- ⁶²R. W. Chan, M. Fu, L. Young, and N. Tirunagari, "Relative contributions of collagen and elastin to elasticity of the vocal fold under tension," *Ann. Biomed. Eng.* **35**(8), 1471–1483 (2007).
- ⁶³R. W. Chan and M. L. Rodriguez, "A simple-shear rheometer for linear viscoelastic characterization of vocal fold tissues at phonatory frequencies," *J. Acoust. Soc. Am.* **124**(2), 1207–1219 (2008).
- ⁶⁴L. Oren, D. Dembinski, E. Gutmark, and S. Khosla, "Characterization of the vocal fold vertical stiffness in a canine model," *J. Voice* **28**(3), 297–304 (2014).
- ⁶⁵P. Shrimpton, "Electron density values of various human tissues: In vitro compton scatter measurements and calculated ranges," *Phys. Med. Biol.* **26**(5), 907–911 (1981).
- ⁶⁶W. Bolch, K. Eckerman, A. Endo, J. Hunt, D. Jokisch, C. Kim, K. Kim, C. Lee, J. Li, N. Petoussi-Hens, T. Sato, H. Schlattl, Y. S. Yeom, and M. Zankl, "ICRP publication 143: Paediatric reference computational phantoms," *Ann. ICRP* **49**(1), 5–297 (2020).
- ⁶⁷A. H. Mendelsohn and Z. Zhang, "Phonation threshold pressure and onset frequency in a two-layer physical model of the vocal folds," *J. Acoust. Soc. Am.* **130**(5), 2961–2968 (2011).
- ⁶⁸See supplementary materials at <https://www.scitation.org/doi/suppl/10.1121/10.0016997> for high-speed video of VF oscillations with nodules of different size and stiffness.
- ⁶⁹V. M. Espinoza, M. Zaňartu, J. H. Van Stan, D. D. Mehta, and R. E. Hillman, "Glottal aerodynamic measures in women with phonotraumatic and nonphonotraumatic vocal hyperfunction," *J. Speech Lang. Hear. Res.* **60**, 2159–2169 (2017).
- ⁷⁰V. M. Espinoza, D. D. Mehta, J. H. Van Stan, R. E. Hillman, and M. Zaňartu, "Glottal aerodynamics estimated from neck-surface vibration in women with phonotraumatic and nonphonotraumatic vocal hyperfunction," *J. Speech Lang. Hear. Res.* **63**(9), 2861–2869 (2020).
- ⁷¹R. J. Baken and R. F. Orlikoff, *Clinical Measurement of Speech and Voice*, 2nd ed. (Singular Thomson Learning, San Diego, CA, 2000).
- ⁷²J. J. Jiang and I. R. Titze, "Measurement of vocal fold intraglottal pressure and impact stress," *J. Voice* **8**, 132–144 (1994).
- ⁷³P. R. Murray and S. L. Thomson, "Vibratory responses of synthetic, self-oscillating vocal fold models," *J. Acoust. Soc. Am.* **132**(5), 3428–3438 (2012).
- ⁷⁴Z. Zhang, "Dependence of phonation threshold pressure and frequency on vocal fold geometry and biomechanics," *J. Acoust. Soc. Am.* **127**(4), 2554–2562 (2010).
- ⁷⁵M. Doellinger and D. A. Berry, "Visualization and quantification of the medial surface dynamics of an excised human vocal fold during phonation," *J. Voice* **20**(3), 401–413 (2006).
- ⁷⁶I. R. Titze and F. Alipour, *The Myoelastic Aerodynamic Theory of Phonation* (National Center for Voice and Speech, Salt Lake City, UT, 2006).
- ⁷⁷R. E. Kania, S. Hans, D. M. Hartl, P. Clement, L. Crevier-Buchman, and D. F. Brasnu, "Variability of electroglottographic glottal closed quotients: Necessity of standardization to obtain normative values," *Arch. Otolaryngol. Head Neck Surg.* **130**(3), 349–352 (2004).
- ⁷⁸J. Lohscheller, J. G. Švec, and M. Döllinger, "Vocal fold vibration amplitude, open quotient, speed quotient and their variability along glottal length: Kymographic data from normal subjects," *Logoped. Phoniatr. Vocol.* **38**, 182–192 (2013).
- ⁷⁹R. C. Scherer, S. Torkaman, B. R. Kucinschi, and A. A. Afjeh, "Intraglottal pressures in a three-dimensional model with a non-rectangular glottal shape," *J. Acoust. Soc. Am.* **128**(2), 828–838 (2010).
- ⁸⁰B. Schneider and W. Bigenzahn, "Influence of glottal closure configuration on vocal efficacy in young normal-speaking women," *J. Voice* **17**(4), 468–480 (2003).
- ⁸¹D. Y. Kim, L. S. Kim, K. H. Kim, M. W. Sung, J. L. Roh, T. K. Kwon, S. J. Lee, S. H. Choi, S. G. Wang, and M. Y. Sung, "Videostrobokymographic analysis of benign vocal fold lesions," *Acta Otolaryngol.* **123**(9), 1102–1109 (2003).
- ⁸²V. Birk, S. Kniesburges, M. Semmler, D. A. Berry, C. Bohr, M. Döllinger, and A. Schützenberger, "Influence of glottal closure on the phonatory process in *ex vivo* porcine larynges," *J. Acoust. Soc. Am.* **142**(4), 2197–2207 (2017).
- ⁸³S. Falk, S. Kniesburges, S. Schoder, B. Jakubaß, P. Maurerlehner, M. Echtermach, M. Kaltenbacher, and M. Döllinger, "3D-FV-FE aeroacoustic larynx model for investigation of functional based voice disorders," *Front. Physiol.* **12**, 616985 (2021).
- ⁸⁴F. G. Dikkers, "Benign lesions of the vocal folds: Clinical and histopathological aspects," Ph.D. thesis, University of Groningen, Groningen, Netherlands, 1994.